Patient-Specific Modeling of Corneal Refractive Surgery Outcomes and Inverse Estimation of Elastic Property Changes

Abhijit Sinha Roy
Cole Eye Institute,
Cleveland Clinic,
Cleveland, OH 44195

William J. Dupps, Jr.[1]
Cole Eye Institute,
Department of Biomedical Engineering,
and Transplant Center,
Surgery Institute,
Cleveland Clinic,
Cleveland, OH;
Department of Biomedical Engineering,
Case Western Reserve University,
Cleveland, OH 44195
e-mail: bjdupps@sbcglobal.net

The purpose of this study is to develop a 3D patient-specific finite element model (FEM) of the cornea and sclera to compare predicted and in vivo refractive outcomes and to estimate the corneal elastic property changes associated with each procedure. Both eyes of a patient who underwent laser-assisted in situ keratomileusis (LASIK) for myopic astigmatism were modeled. Pre- and postoperative Scheimpflug anterior and posterior corneal elevation maps were imported into a 3D corneo-scleral FEM with an unrestrained limbus. Preoperative corneal hyperelastic properties were chosen to account for meridional anisotropy. Inverse FEM was used to determine the undeformed corneal state that produced <0.1% error in anterior elevation between simulated and in vivo preoperative geometries. Case-specific 3D aspheric ablation profiles were simulated, and corneal topography and spherical aberration were compared at clinical intraocular pressure. The magnitude of elastic weakening of the residual corneal bed required to maximize the agreement with clinical axial power was calculated and compared with the changes in ocular response analyzer (ORA) measurements. The models produced curvature maps and spherical aberrations equivalent to in vivo measurements. For the preoperative property values used in this study, predicted elastic weakening with LASIK was as high as 55% for a radially uniform model of residual corneal weakening and 65% at the point of maximum ablation in a spatially varying model of weakening. Reductions in ORA variables were also observed. A patient-specific FEM of corneal refractive surgery is presented, which allows the estimation of surgically induced changes in corneal elastic properties. Significant elastic weakening after LASIK was required to replicate clinical topographic outcomes in this two-eye pilot study. [DOI: 10.1115/1.4002934]

Keywords: cornea, computational model, laser-assisted in situ keratomileusis (LASIK), hysteresis, biomechanics

1 Introduction

Laser-assisted in situ keratomileusis (LASIK), the most commonly performed refractive surgery, involves the creation of a lamellar flap followed by patterned photoablation of the underlying stroma. In a recent large-scale review of LASIK outcomes over a decade-long study period, most patients (95%) were highly satisfied with their outcome. However, 5% expressed dissatisfaction with the surgical outcome based on the low quality of life scores that were attributed, in part to refractive regression, poor night vision, and residual refractive error [1]. Modern excimer laser systems provide options for wavefront-guided ablation profiles that, along with other technological advances such as eye tracking, have reduced the tendency toward the induction of higher order aberrations (HOAs) compared with previous conventional LASIK technologies [2–5]. However, the predictability of spherocylindrical refractive outcomes and the induction of HOAs are persistent multifactorial problems that cannot be completely explained by nonidealities in the laser-tissue interaction [6–10], nor can they be fully addressed with ablation profiles based solely on preoperative wavefront data [4,5,8].

Alterations in the biomechanical state of the cornea have been proposed to affect the optical outcome of LASIK [7–9]. Conceptual biomechanical models presume a reduction in the material strength of the cornea, owing to the combined effects of photoablative lamellar disruption and flap creation [7,8], but the magnitude of elastic weakening remains unknown. Quantification of this weakening is important not only in relation to the unintended biomechanically mediated spherocylindrical and higher order optical effects [3–5,11,12] but also because of a presumed role in the pathogenesis of postsurgical corneal ectasia.

Previously, we introduced a whole-eye 2D finite element model (FEM) and evaluated the sensitivity of simulated LASIK outcomes to preoperative corneal hyperelastic properties [13]. The model, like others before it, made no allowance for a reduction in intrinsic material properties after surgery. Most reported FE models of the preoperative and postoperative cornea have incorporated this simplification and others that limit their ability to account for clincially relevant astigmatic optical effects and higher order aberrations. These include analytical surfaces rather than clinically derived topographies and 2D models that do not account for 3D corneal asymmetry and asphericity [13–17]. Furthermore, ablation profiles in previous studies [15] have been derived from the original spherical Munnerlyn equation [18] without accounting for astigmatic patterns or aspheric profiles in modern lasers [19,20]. Another limitation of some models is the use of a fixed or restrained limbus boundary condition, which may lead to corneal deformations that are inconsistent with in vivo behavior [21–23]. Thus, an unrestrained limbus using a whole-eye model [13] or a

[1]Corresponding author.

Contributed by the Bioengineering Division of ASME for publication in the JOURNAL OF BIOMECHANICAL ENGINEERING. Manuscript received February 11, 2010; final manuscript received October 11, 2010; accepted manuscript posted November 2, 2010; published online December 22, 2010. Assoc. Editor: Victor H. Barocas.

Table 1 Preoperative and post-LASIK characteristics of the right and left eyes

	Right eye		Left eye	
	Preoperative	Post-LASIK	Preoperative	Post-LASIK
Manifest refraction (D)	−5.00+0.75 ×120 deg	−0.25+0.50 ×20 deg	−5.50+0.50 ×87 deg	−0.25+0.50 ×165 deg
Best corrected visual acuity	20/20	20/25	20/20	20/25
CCT (μm)	603	-	604	-
SimK (D)	41.25/42.87 at 112 deg	38.50/39.00 at 160 deg	42.37/43.50 at 78 deg	38.00/38.50 at 90 deg
CH (mm Hg)	10.7	7.5	10.5	8.3
CRF (mm Hg)	10.5	7.8	10.3	8.0
IOP_g (mm Hg)	15.3	15.1	15.3	14.5
IOP_{cc} (mm Hg)	15	18.7	14.8	16.5

comparable corneoscleral model [15] is preferable in predictive FEMs for approximating in vivo surgical outcomes such as spherocylindrical refractive power and HOA.

The aims of this study were to (1) develop a computationally efficient 3D in vivo (patient-specific) corneoscleral model using clinical corneal geometry, (2) to compare computational corneal power predictions to 1 week in vivo surgical outcomes of myopic LASIK in a two-eye clinical pilot study, and (3) to estimate corneal elastic property changes associated with each procedure. A secondary aim was to assess the sensitivity of the model to two different schemes for corneal elastic property change within the residual bed of the treated zone: a uniform reduction and a nonuniform reduction as a function of local ablation depth.

2 Methods

2.1 Geometry. The right and left eyes of a 35 year old female patient who underwent LASIK for myopia with astigmatism at the Cleveland Clinic Cole Eye Institute were investigated retrospectively under an Institutional Review Board (IRB) approval for chart review research (Cleveland Clinic IRB No. 07-305). Preoperative and postoperative clinical characteristics are provided in Table 1. The 3D model of the cornea was constructed using tomographic data from a commercial anterior segment imaging system (Pentacam, Oculus Optikgeräte GmbH, Germany). The x, y, and z coordinates from the elevation maps of the anterior and posterior surfaces were interpolated using orthogonal Zernike polynomials up to the sixth order, having 28 terms and with a 5 mm normalization radius. The root-mean-square errors, defined as the square root of the mean of the sum of the difference between the in vivo and Zernike predictions, for the elevation data were 1.65 μm and 1.32 μm for the right and left eyes, respectively. The interpolated elevation data (x, y, and z) were used to obtain a 3D surface using a commercial computer aided drafting (CAD) package (PROENGINEER WILDFIRE, PTC, Needham, MD). Each point along a radius was connected by a cubic spline to form a curvilinear edge in 3D. Multiple edges that form the shape of a corneal surface were then blended to obtain a 3D surface for the anterior and posterior cornea. These surfaces (anterior and posterior) were then joined at the limbus to form a 3D solid, representing the in vivo pre-LASIK cornea. To simulate an unrestrained limbus, a scleral shell was extended from the cornea to an axial length of 3.5 mm. The posterior borders of the sclera were restrained completely. The posterior surfaces of the cornea and sclera were loaded with IOP_{cc} (Table 1) obtained from the ocular response analyzer (ORA). IOP_{cc} is the cornea compensated intraocular pressure and is considered to be less sensitive to changes in the corneal biomechanical properties and thickness after LASIK compared with the Goldmann applanation [24–28].

In the clinical setting, corneal topography is measured at a specific intraocular pressure (IOP) and is distinct from the unloaded shape that would be obtained at an IOP of 0 mm Hg. To solve for the undeformed state, a custom inverse model was developed using the commercial finite element (FE) analysis package ABAQUS (Simulia Inc.) and PYTHON scripting language. In the inverse model, initial estimates of the unloaded shapes of the cornea and sclera were loaded to clinical IOP and then compared with the in vivo shape. The coordinates of the unloaded shape was then corrected based on the difference between the coordinates of the in vivo geometry and the FEM prediction. The resulting unloaded shape was then loaded again to the same IOP. This procedure was repeated until a user-specified tolerance of 0.1% (the difference between the coordinates of two FEM results from successive simulations of loading the corneo-scleral model from zero to in vivo IOP) was achieved. The mesh for each model consisted of linear, eight node 3D hexahedral elements.

2.2 Material Properties. The cornea is an anisotropic tissue that shows stress stiffening at higher strains due to a complex collagen fibrillar distribution. Fibril-oriented material properties have been used in some recent FEM studies [14,16,17], while orthotropic linear elastic material properties have been used in others [15]. In this study, a spatially dependent, hyperelastic material property formulation has been used to simulate the elastic properties of the cornea. Elsheikh et al. [29] measured corneal elastic properties along the horizontal, oblique, and vertical meridians of ex vivo human corneas and observed that the vertical and oblique meridian were most and least stiff, respectively (Fig. 1(a)). While Elsheikh et al. [29] used uniaxial strip testing to quantify properties along meridians, similar meridional differences were demonstrated experimentally by Dupps et al. [30], using a validated nondestructive ultrasound based method of wave speed measurement [31] in intact corneas with physiologic whole-globe boundary conditions. For the purposes of the current study, each of the experimentally derived stress versus strain curves (Fig. 1(a)) were fit to a reduced polynomial material model, $W = C_{10}(I_1-3)+C_{20}(I_1-3)^2$, where W is the strain energy potential and I_1 is the strain invariant. C_{10} and C_{20} are hyperelastic constants obtained from the fitting of the experimental stress versus strain data and were determined for each of the three meridia. The magnitude of C_{10} and C_{20} along the other meridia were then interpolated using sinusoidal functions (one each for C_{10} and C_{20}), $C = a \times \sin^2(\text{theta}) + b \times \sin(\text{theta}) + c$, where theta is the meridian and a, b, and c are the constants obtained from the regression. At theta=0 (the horizontal meridian), C obtained from the above function will yield the same hyperelastic constant values C_{10} and C_{20} obtained for the horizontal meridian ex vivo data. A sinusoidal function was chosen to ensure a smooth gradient in C_{10} and C_{20} across all meridians of the cornea. The reduced polynomial form and the sinusoidal function were implemented using user-defined subroutines in ABAQUS. The sclera was also modeled using the reduced polynomial form as an isotropic and hyperelastic material. Scleral elastic properties were assumed to be three times the stiffness of the vertical meridian of the cornea [13].

2.3 Ablation Profile. The patient underwent wavefront-optimized (Allegretto Wave® Eye-Q Excimer Laser System, Alcon Laboratories, Fort Worth, TX) ablation for myopia with astigmatism in both eyes. Details of the ablation parameters and flap thickness are provided in Table 2. The mathematical formulation

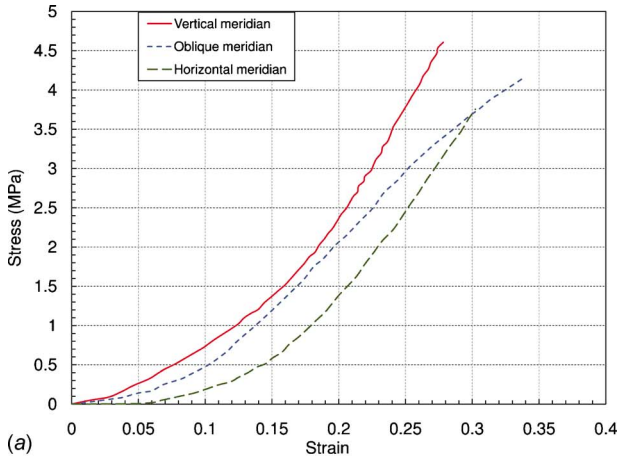

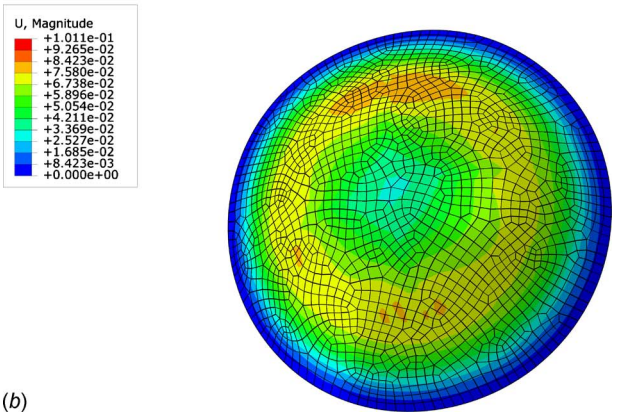

Fig. 1 (*a*) **Stress-strain relationships along three meridia obtained from the experimental data of Elsheikh et al. [29] and** (*b*) **a 3D corneoscleral model with finite element mesh and a superimposed map of displacements resulting from loading the undeformed pre-LASIK model (determined from inverse FEM) to clinically measured preoperative IOP. The paracentral and peripheral cornea exhibits greater displacements than the central zone (in mm).**

for calculating the ablation depth as a function of the radius and meridian has been described for an aspheric profile [19] and was used to generate the initial ablation profile for the programmed treatments. The ablation depth function was then modified to account for loss of ablation efficiency from a non-normal incidence of the laser beam away from the center of the cornea [9]. The ablation depth in millimeters was subtracted from the corresponding z coordinate of the anterior surface of the unloaded corneal shape obtained from inverse modeling, as described previously. The resulting unloaded shape was then loaded to the clinically measured IOP_{cc} obtained 1 week after surgery, and the post-LASIK geometry was calculated in ABAQUS and compared with 1 week clinical geometry outcomes.

Table 2 LASIK treatment parameters for the left and right eyes

	OD	OS
Programed correction (D)	−4.75+0.75 ×120 deg	−5.25+0.50 ×87 deg
Optical zone/total ablation zone diameter (mm)	6.5/9	6.5/9
Programed flap thickness (μm)	100	100
Flap thickness by ultrasound subtraction pachymetry (μm)	129	115
Programed central ablation depth (μm)	71	78

2.4 Estimation of Magnitude of Elastic Weakening After LASIK. To model the effect of tissue removal on corneal material properties in post-LASIK cornea, the elastic properties (C_{10} and C_{20}) were reduced through the full thickness encompassed by the ablation zone diameter (including the region of the flap and the residual stromal bed) to a magnitude that produced the best three-dimensional match to the in vivo postoperative anterior surface axial power. It was assumed that the elastic properties of the flap region were the same as the elastic properties of the postoperative residual corneal bed. The parameter used for comparison was the ratio of axial power calculated by FEM to the axial power in vivo. Thus, the ratio would be 1 if axial power calculated by FEM equals the axial power in vivo at a given point on the anterior surface. It is most likely that the elastic weakening following LASIK is nonhomogenous (spatially varying), though the exact distribution of variation is not known. Therefore, two methods were adopted to model the weakened cornea post-LASIK:

(i) *Uniform reduction*. In the central 6.5 mm optical zone, the hyperelastic constants (C_{10} and C_{20}) were reduced through the postoperative corneal thickness by a constant factor F in all meridians. Therefore, the post-LASIK elastic properties of the cornea were modeled as $C_{10\text{-post}}=C_{10\text{-pre}}\times F$. This approach assumed negligible elastic property changes in the transition zone peripheral to the optical zone.

(ii) *Radially nonuniform reduction*. This method assumes that a greater ablation depth produces a greater local reduction in elastic property coefficients. In the central 9 mm zone encompassing both the optical and transition zones, elastic properties were reduced in proportion to the ablation depth at each point. The factor that was multiplied with the preoperative elastic property coefficients to determine the postoperative local coefficients was given by $F=(\Delta E-1)\times(t/CAD)+1$, where CAD is the central ablation depth, t is the ablation depth at a particular point, and ΔE is the fraction of the original elastic coefficients to which the postoperative elastic coefficients were reduced at the center of ablation. With this construct, the maximum elastic weakening was located at the center of the ablation zone and decreased progressively toward the peripheral cornea.

In the above methods, the change in elastic properties was calculated based on pre-LASIK properties obtained by Elsheikh et al. [29] who used specimens from older patients. Since the true elastic properties of the eyes used in the present study were unknown and the patients in this study were younger than those tested by Elsheikh et al. [29], a simple sensitivity analysis was performed by decreasing the elastic properties of the cornea and sclera by 25% from the baseline values and maintaining a scleral-corneal elasticity ratio of 3:1.

Four replicate ORA measurements for each eye and at each time point were obtained before and after LASIK. Estimated reductions in elastic properties using the uniform and nonuniform reduction methods were compared with changes in corneal hysteresis (CH) and corneal resistance factor (CRF).

2.5 Computation of Spherical Aberration of the Anterior Surface of Cornea. The spherical aberration of the in vivo and FEM anterior corneal surfaces was compared across a central 10 mm diameter zone to include central, paracentral, and peripheral corneal effects. A diameter of 10 mm was chosen to include the entire ablation zone of a 9 mm diameter and to avoid numerical noise associated with Zernike polynomials at the edges of the analysis zone. The mathematical formulation to calculate the ab-

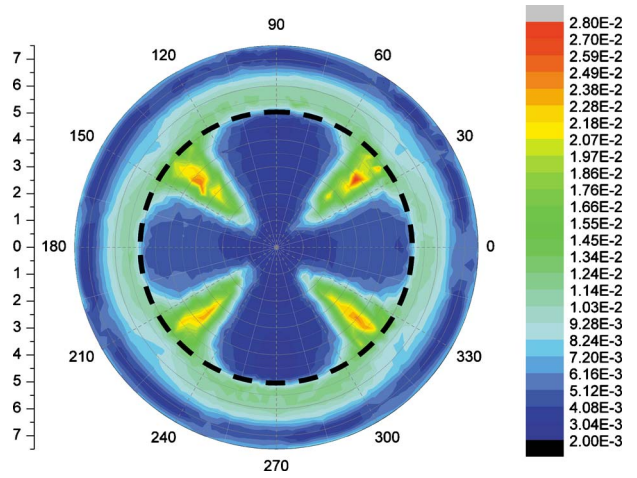

Fig. 2 Maximum principal strain under applied IOP. The black dashed circle demarcates the corneal border. Differences in the strain are due to encoding experimentally derived meridional variations in hyperelastic properties of the cornea. Peak strains are predicted by the FEM along the oblique meridia.

erration at any point on the anterior surface of the cornea was previously described [32]. The aberrations of the entire 10 mm zone were analyzed using Zernike polynomials. The fourth order term (C_{40} using the double index scheme) in the Zernike analysis was designated as the spherical aberration [32].

3 Results

Comparisons of in vivo and FEM optical predictions are presented as ratios of the axial power predicted by FEM to the axial power in vivo at the same location on the anterior cornea surface. In Fig. 1(*b*), a displacement contour is shown along with the finite element mesh for the right eye when stressed with IOP_{cc} from the unloaded to the in vivo preoperative state. The central corneal displacement ($\sim$33 μm) was much lower than the displacement of the paracentral ($\sim$55 μm) and peripheral cornea. This displacement distribution is consistent with results from a previous whole-eye analysis [13]. Fig. 2 shows the maximum principal strain when the model is loaded with physiologic IOP. The maximum and minimum strains were localized along the oblique and vertical meridia, respectively. At the limbus and surrounding sclera, the strain distribution was more circumferentially oriented due to the assumed isotropy in these regions. This strain pattern was consistent with past studies that have used preferred collagen fibril orientation material models [14,16,17]. The means of replicate CH, CRF, IOP_g (Goldmann-equivalent IOP), and IOP_{cc} measurements are reported in Table 1 for the pre- and post-LASIK states.

3.1 Right Eye Geometric Results. The anterior surface axial power measured clinically prior to LASIK is shown in Fig. 3(*a*). Figure 3(*b*) depicts the ratio of the preoperative axial power derived from inverse FEM to the preoperative in vivo axial power. In Fig. 3(*c*), the ratio map describes the agreement of the FEM-derived axial power to the in vivo axial power 1 week after LASIK, with the assumption that no change in elastic properties occurs. Figure 3(*d*) shows a similar plot of the ratio, with the assumption that LASIK causes a uniform reduction in elastic properties to 0.45 times their preoperative value in the central 6.5 mm optical zone. Table 3 summarizes each model's fit to the in vivo data as the mean ratio $\pm$ sd for the central 3 mm zone, the 3–6 mm diameter zone, and the 6–10 mm diameter zone. The mean agreement of the preoperative inverse model prediction to the clinical axial power map is within 0.5%, with a standard deviation of less than 0.15%. This implies that the no-load (zero IOP) configuration of the corneo-scleral model predicted by the inverse model, when loaded to physiological IOP, produces a corneal curvature equivalent to patient-specific in vivo measurements.

In the post-LASIK case, with the assumption of unchanged corneal elastic properties, the mean value of the ratio was 0.9773 ± 0.0145 (sd) in the central 3 mm diameter zone. Recall that the post-LASIK FEM geometry is derived by the application of the simulated case-specific ablation to the undeformed model and loading of the resulting geometry to the clinical IOP measured after LASIK. The FEM predicted a slightly flatter cornea (ratio <1) than the in vivo post-LASIK outcome. When the elastic properties in the optical zone were uniformly reduced to a level that minimized model error (0.45 times the preoperative value), the average ratio in the central 3 mm diameter zone increased to 1.0012 ± 0.015. In the paracentral zone (3–6 mm), there was an improvement in the mean value of the ratio from 0.9888 to 1.0092, with the reduction in elastic properties. The results indicate that a 55% reduction $((1-0.45)\times 100)$ in corneal elastic properties within the diameter of the optical zone is required to reproduce the in vivo topographic outcome.

In the nonuniform reduction method, it was assumed that the magnitude of elastic property change is a function of ablation depth, with the maximum reduction at the center of a myopic ablation. The optimization routine described in Sec. 2 resulted in a nonuniform elastic property reduction model with $\Delta E = 0.35$ (representing a 65% central reduction in elastic properties relative to preoperative properties) for the right eye (Fig. 5(*a*)). The distribution of elastic property reduction was defined by the ablation profile. For $\Delta E = 0.35$, the mean value of the ratio in the central 3 mm zone was 1.0006 ± 0.014 (mapped in Fig. 5(*c*) and summarized by zone in Table 3). Mean values of the ratio in the other zones were similar to those obtained with a uniform 55% reduction in elastic properties. Table 3 also lists the values of the ratios $\pm$ sd for the conditions where the cornea and sclera elastic properties were decreased by 25%. Optimization yielded a weakening by 50% and $\Delta E = 0.40$, with the uniform and nonuniform model, respectively, having only a 5% difference from the original material property assumption.

3.2 Left Eye Geometric Results. Figure 4(*a*) shows the in vivo axial power before LASIK. Figure 4(*b*) depicts the ratio of the preoperative axial power derived from the inverse FEM to the preoperative in vivo axial power. In Fig. 4(*c*), the ratio map describes the agreement of the FEM-derived axial power to the in vivo axial power 1 week after LASIK, with the assumption that there are no changes in elastic properties. Figure 4(*d*) shows a similar plot of the ratio, with the assumption that LASIK reduces the elastic properties of the central 6.5 mm optical zone to 0.6 times the preoperative values. Table 4 summarizes each model's fit to the in vivo data as the mean ratio $\pm$ sd for the central 3 mm zone, the 3–6 mm diameter zone, and the 6–10 mm diameter zone. The mean agreement of the preoperative inverse model prediction to the clinical axial power map is within 0.5%, with a standard deviation of less than 0.2%. As with the right eye, the zero-load configuration of the corneo-scleral model predicted by the inverse FEM routine, when loaded to physiological IOP, produced a corneal curvature equivalent to the in vivo measurements.

In the post-LASIK case, with the assumption of unchanged elastic properties, the mean value of the ratio was 0.9887 ± 0.021 in the central 3 mm diameter zone. As in the right eye, the FEM overestimated the flattening effect of LASIK when corneal elastic properties were assumed to be unaffected by the surgery. When the elastic properties in the optical zone were uniformly reduced to a level that minimized model error (0.6 times the preoperative values), the average ratio in the central 3 mm diameter zone increased to 1.0002 ± 0.02. In the paracentral zone (3–6 mm), there was an improvement in the mean value of the ratio from 0.9888 to 1.0092, with this reduction in stiffness, and differences of less

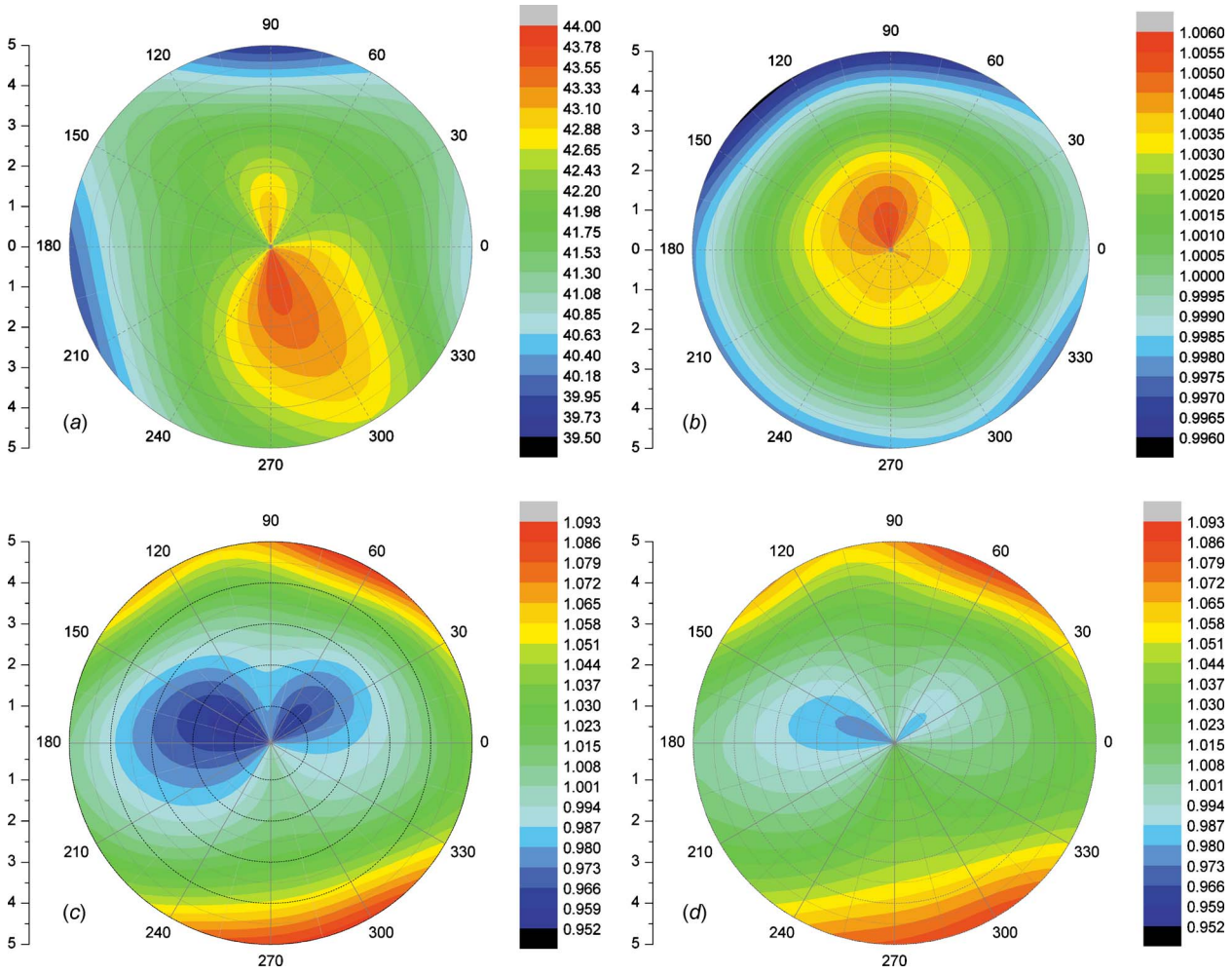

Fig. 3 (*a*) **Clinical preoperative anterior axial power map of the right eye in diopters,** (*b*) **map of the ratio of the preoperative axial power predicted from the inverse FEM to the in vivo axial power for the right eye,** (*c*) **maps of the ratio (post-LASIK FEM/post-LASIK in vivo) of the postoperative anterior axial power assuming there was no change in elastic properties after LASIK, and** (*d*) **uniformly reduced elastic properties throughout the optical zone (diameter of 6.5 mm) after LASIK in the right eye**

Table 3 Average ratios of FEM-derived/in vivo axial power in different zones of the right cornea before and after LASIK, with assumptions of no surgically induced reduction, uniform reduction throughout the optical zone, and ablation-depth dependent reduction throughout the optical and transition zones. The table also lists the values of the ratios when the elastic properties of the cornea and sclera were reduced by 25%.

	Average values of ratio ± sd				Average values of ratio ± sd		
	Pre-LASIK	Post-LASIK			Post-LASIK cornea and sclera: 25% weaker		
Analysis diameter (mm)	Inverse model	No elastic property reduction	Uniform elastic property reduction (55%)	Nonuniform elastic property reduction (ΔE=0.35)	No elastic property reduction	Uniform elastic property reduction (50%)	Nonuniform elastic property reduction ΔE=0.40
0–3	1.0041 ± 0.0006	0.9773 ± 0.0145	1.0012 ± 0.0150	1.0006 ± 0.0141	0.9831 ± 0.0143	1.0074 ± 0.0147	1.004 ± 0.0138
3–6	1.0028 ± 0.0006	0.9888 ± 0.0154	1.0092 ± 0.0153	1.0055 ± 0.0145	0.9941 ± 0.015	1.0151 ± 0.015	1.0119 ± 0.0143
6–10	0.9997 ± 0.0013	1.0258 ± 0.0256	1.0348 ± 0.0219	1.0318 ± 0.0200	1.0306 ± 0.0256	1.0396 ± 0.0220	1.0368 ± 0.0224

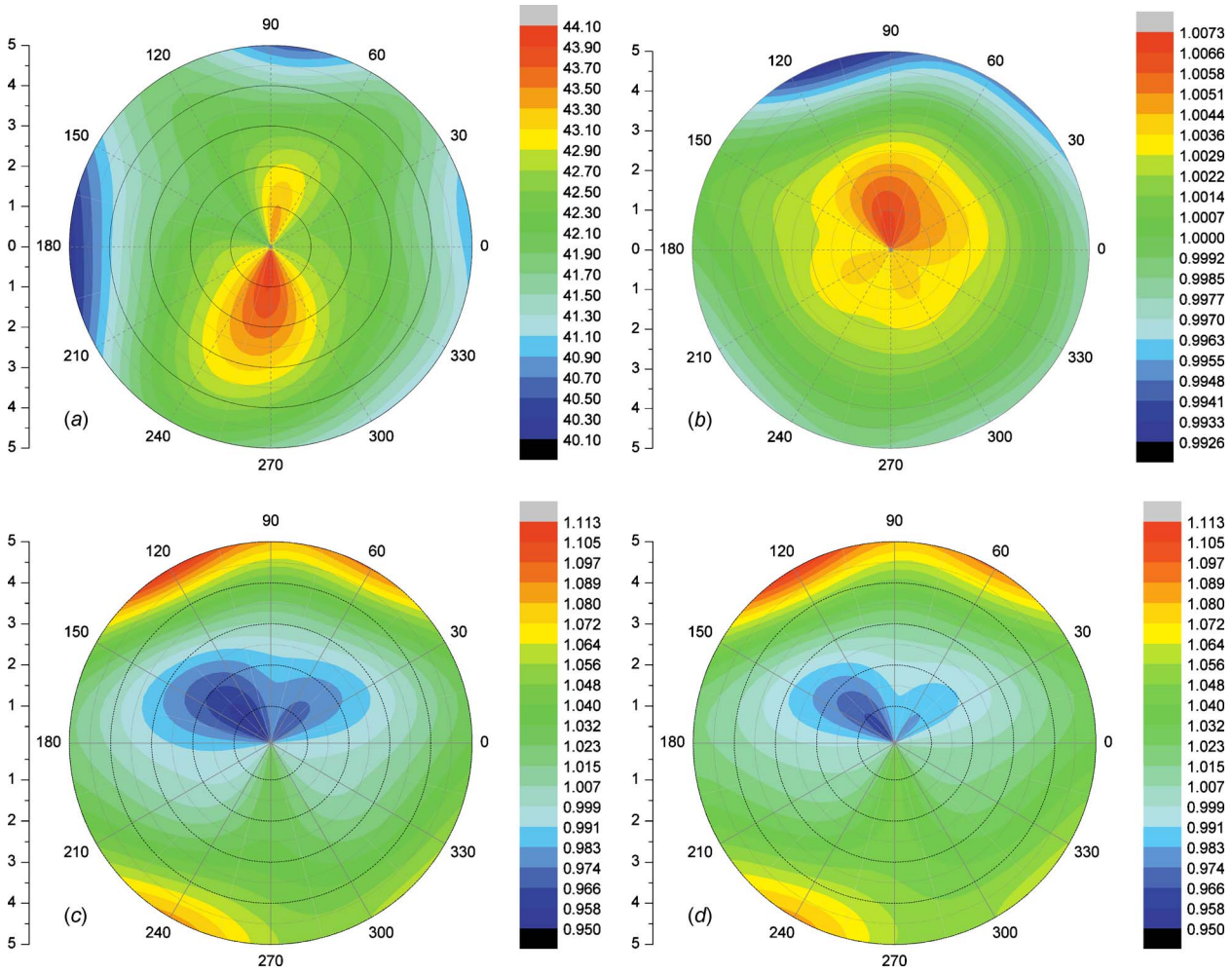

Fig. 4 (*a*) **Clinical preoperative anterior axial power map of the left eye in diopters,** (*b*) **map of the ratio of the preoperative axial power predicted from the inverse FEM model to the in vivo axial power for the left eye,** (*c*) **maps of the ratio (post-LASIK FEM/post-LASIK in vivo) of the postoperative anterior axial power assuming there was no change in elastic properties after LASIK, and** (*d*) **uniformly reduced elastic properties throughout the optical zone (diameter of 6.5 mm) after LASIK in the left eye**

Table 4 Average ratios of FEM-derived/in vivo axial power in different zones of the left cornea before and after LASIK, with assumptions of no surgically induced reduction, uniform reduction throughout the optical zone, and ablation-depth dependent reduction throughout the optical and transition zones. The table also lists the values of the ratios when the elastic properties of the cornea and sclera were reduced by 25%.

	Average values of ratio ± sd				Average values of ratio ± sd		
	Pre-LASIK	Post-LASIK			Post-LASIK cornea and sclera: 25% weaker		
Analysis diameter (mm)	Inverse model	No elastic property reduction	Uniform elastic property reduction (40%)	Nonuniform elastic property reduction (ΔE=0.50)	No elastic property reduction	Uniform elastic property reduction (40%)	Nonuniform elastic property reduction ΔE=0.50
0–3	1.0044 ± 0.0011	0.9887 ± 0.0205	1.0002 ± 0.0210	1.0005 ± 0.0205	0.9891 ± 0.0201	1.0047 ± 0.0208	1.0013 ± 0.0202
3–6	1.003 ± 0.0008	0.9983 ± 0.0176	1.0083 ± 0.0177	1.0083 ± 0.0173	0.9992 ± 0.0173	1.0129 ± 0.0175	1.0102 ± 0.0169
6–10	0.9995 ± 0.0017	1.0326 ± 0.0210	1.0375 ± 0.0213	1.0363 ± 0.0211	1.0362 ± 0.0244	1.0400 ± 0.0220	1.036 ± 0.0218

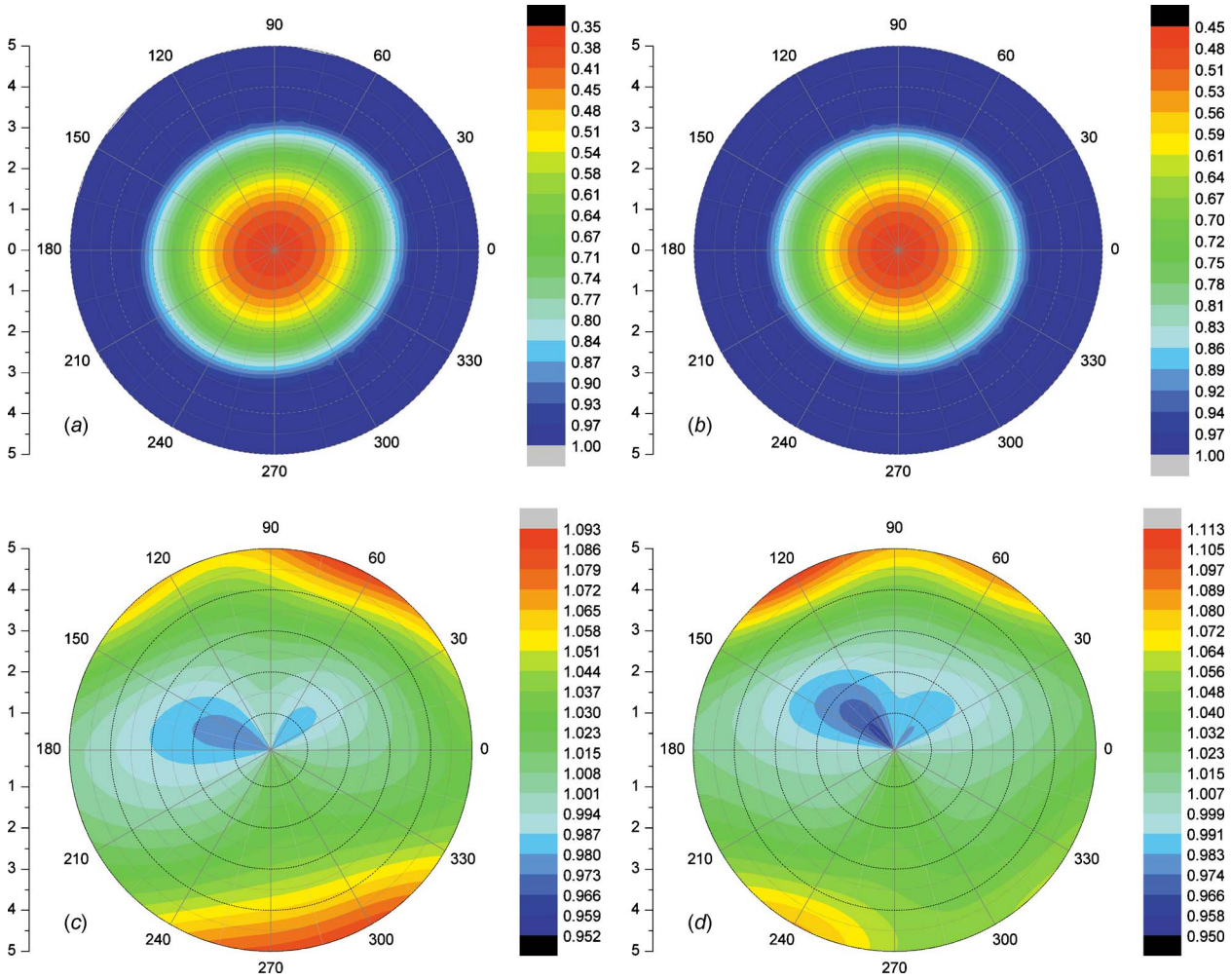

Fig. 5 Patterns of radially nonuniform reduction in elastic properties in (*a*) the right eye (ΔE=0.35) and (*b*) the left eye (ΔE=0.5), where ΔE represents the factor multiplied with the preoperative property values to give the postoperative values and was determined for each case through an optimization process designed to maximize agreement between clinical and simulated postoperative anterior surface axial powers. Ratio of the predicted to actual anterior axial power (post-LASIK FEM/post-LASIK in vivo), assuming an ablation-depth dependent reduction in elastic properties within the ablation zone for (*c*) the right eye and (*d*) the left eye.

than 1% were seen in the peripheral zones between the no-change and uniform-change stiffness models. The results indicate that in the left eye, a 40% reduction $((1-0.60)\times 100)$ in corneal elastic properties within the diameter of the optical zone was required to reproduce the clinical topographic changes.

With a nonuniform post-LASIK stiffness reduction, the optimization produced ΔE=0.5, representing a 50% maximum central reduction in elastic properties relative to preoperative properties for the right eye (Fig. 5(*b*)). The mean value of the axial power ratio in the central 3 mm zone was 1.0005 ± 0.0205 (mapped in Fig. 5(*d*) and summarized by zone in Table 4). Mean values of the ratio in the other zones were similar to those obtained with a uniform 40% elastic property reduction. Table 4 also lists the values of the ratios ± sd for the conditions where the cornea and sclera elastic properties were decreased by 25%. Optimization of the FEM prediction to the post-LASIK outcome yielded a weakening by 40% and ΔE=0.50 with the uniform and nonuniform models, respectively. Unlike the right eye, altering the cornea and sclera properties did not alter the estimate of corneal weakening post-LASIK.

3.3 Spherical Aberration: Pre- and Post-LASIK. Spherical aberration of the cornea for both pre- and post-LASIK was evaluated over a diameter of 10 mm. Figure 6(*a*) shows the spherical aberration in right eye before and after LASIK. LASIK caused an increase in spherical aberration from 0.011 μm to 0.017 μm in vivo. The FEM predicted an increase in spherical aberration from 0.012 μm to 0.018 μm when there was no change in elastic properties of the cornea after LASIK. With the nonuniform reduction model, the post-LASIK aberration predicted by the FEM increased slightly to 0.019 μm. Figure 6(*b*) shows the spherical aberration in the left eye before and after LASIK. Similar results for spherical aberration were obtained for the left eye. The change in spherical aberration predicted by the FEM with ablation-depth dependent reductions in elastic properties was similar to that predicted by a uniform reduction in elastic properties. It should be noted that in all simulations, the depth of the tissue is removed and the flap thickness itself undergoes a negligible change as the cornea is loaded from zero to physiological IOP in the FEM and therefore does not contribute significantly to curvature change.

4 Discussion

In this study, we presented a novel set of FEM methods for a patient-specific computational simulation of corneal refractive surgery and performed a pilot comparison of model predictions to in vivo LASIK outcomes. The model allows an analysis of the biomechanical changes associated with a specific LASIK treat-

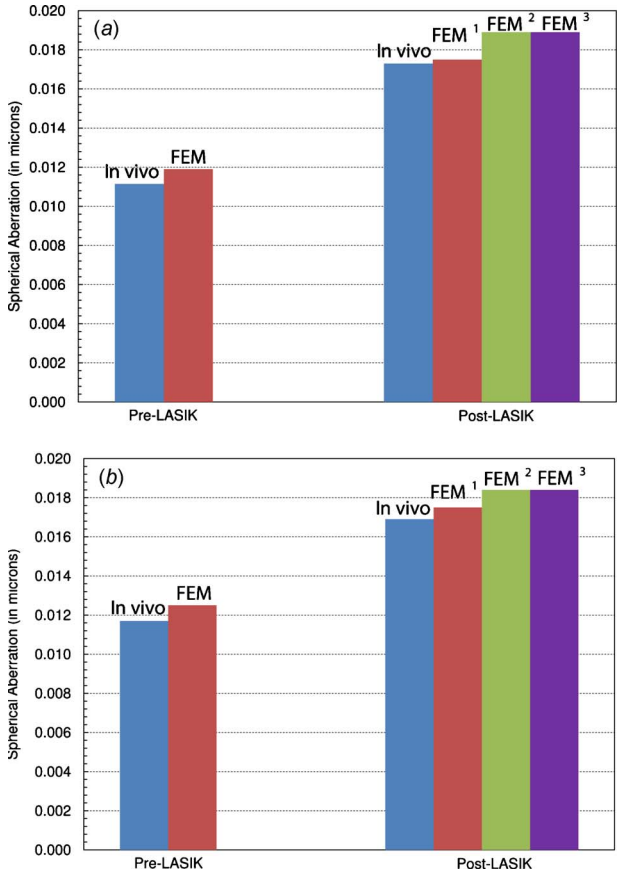

Fig. 6 Comparison of the corneal first-surface spherical aberration calculated from in vivo measurement and FEM prediction for (*a*) the right eye and (*b*) the left eye before and after LASIK: FEM preoperative, FEM[1] postoperative (unchanged elastic properties), FEM[2] postoperative (uniform reduction in elastic properties), and FEM[3] postoperative (nonuniform reduction in elastic properties)

ment plan and their impact on the accuracy of the postoperative optical result. In addition, the model was used to estimate the magnitude of corneal elastic property reductions based on clinical topographic changes between the preoperative and 1 week postoperative examinations. In both eyes, a reduction in corneal elastic properties or weakening of the cornea from the preoperative state resulted in more accurate axial power estimates by the FEM compared with in vivo. These results suggest that the anterior corneal flattening associated with a myopic correction is overestimated if elastic properties are assumed to be as high after surgery as before surgery; conversely, weakening of the cornea, which favors less biomechanical flattening by allowing more forward-directed central corneal displacement after LASIK, is required to produce the best match to the clinical response. The tendency toward overcorrection due to excessive biomechanical flattening with stiff corneas and undercorrection in corneas with lower elastic properties is consistent with the results from our previous whole-eye model of LASIK [13] and supports the hypothesis that a myopic undercorrection may be a clinical marker of weaker corneal elastic properties.

The current approach improves upon previous FEM-based studies that have not incorporated patient-specific clinical measurements of IOP and corneal geometry (including pan-corneal thickness data), have not included the corneo-scleral limbus, have not modeled the effects of corneal meridional elastic property variation, have not accounted for nonidealities in photoablative efficiency during ablation, or have not allowed for a change in corneal elastic properties after LASIK. This study combines the relevant patient-specific clinical information into a model in which a specific surgical algorithm can be simulated to predict the postoperative outcome and to determine the magnitude of elastic property change within the treatment zone, which is required to achieve the best fit to actual clinical outcome. The ablation depth dependent reduction yielded similar optical outcomes after LASIK compared with a uniform reduction method (Tables 3 and 4). It is likely that the changes in elastic properties after LASIK are heterogeneous since ablation depth varies spatially according to the ablation profile. The ability of the nonuniform elastic property reduction method to replicate in vivo outcomes in this pilot study strongly supports this mathematical approach to expressing spatial elastic property change as a function of LASIK ablation parameters in future studies.

Previous FEM studies have not attempted to quantify patient-specific changes in corneal elastic properties after refractive surgery with ORA. Recent clinical studies with the ORA have shown that both CH and CRF decrease after LASIK [33–37]. While CH and CRF capture aspects of ocular biomechanical behavior that are not simple equivalents of elastic modulus [38,39], these studies support the notion of decreased corneal elastic properties after LASIK. In this study, despite similar attempted refractive corrections and similar preoperative CH and CRF values in both eyes, CH decreased by 30% in the right eye and 21% in the left, and CRF decreased by 26% in the right eye and 22% in the left. The FEM results also suggested an asymmetric material property response with a greater weakening of the right eye (55%) than the left (40%), with the baseline pre-LASIK properties. Both findings suggest that the right eye underwent a greater amount of weakening. Moderate to weak correlations have been found between CH and CRF and the change in central corneal thickness (CCT) [26,34,35] or ablation volume [40] in myopic surgery. Deeper ablations and thicker flaps presumably result in greater reductions in corneal elastic properties due to the severance of a proportionate number of collagen lamellae [8,41]. Though symmetric 100 μm thick flaps were attempted with the femtosecond laser, an unintended 14 μm difference in ultrasonically measured central flap thickness (Table 2) between the eyes could be a factor influencing the differential response to similar LASIK procedures. The role of CH and CRF as surrogates for classical elastic properties in computational modeling is unclear and requires further investigation.

This study incorporates spatially varying elastic structures of the cornea using data from ex vivo uniaxial tests at different meridians. Dupps et al. used a nondestructive method to measure the surface ultrasound wave speed along the horizontal and vertical meridians of the cornea in whole-eye human donor globes [30]. The wave speed was significantly higher along the vertical meridian than the horizontal meridian. This finding is similar to the uniaxial test observations reported by Elsheikh et al. [29] but with an in situ corneal configuration with physiologic boundary conditions, stressed with physiologic IOP, and subject to biaxial stretching. The same surface wave technique was subsequently validated to be nearly linearly proportional to the elastic modulus measured by extensiometry [31]. While these observations do not eliminate the possibility of error in the translation of uniaxial test to in situ behavior, they do suggest that the spatial variation of corneal elastic properties is preserved to some degree under both experimental conditions and that the modeling error associated with the extrapolation is likely to be lower as a result. Further, cohesive tensile strength measurements in human corneas after flap creation have suggested a mean reduction in one analog of corneal elastic strength of 72%, though variability was noted [42]. Our estimates of material property reduction in this model are similar, though perhaps lower due to the fact that flap thicknesses in the previous study [42] were greater than the femtosecond laser flaps modeled here. This provides an experimental validation of the magnitude of elastic property change estimated by the present FEMs. The sensitivity analysis where the elastic properties of the cornea and

sclera were reduced keeping the cornea-sclera elasticity ratio constant suggests that at least in these two cases, the model is relatively insensitive to the pre-LASIK hyperelastic property estimates. The model still predicted a greater degree of weakening in the right eye than the left when a lower range of elastic property coefficients (corneal and sclera properties reduced by 25%) were tested.

This study utilizes ex vivo measurements of spatial corneal elastic properties to estimate the changes in corneal elastic property in both eyes. This study also treats the effects of flap creation, photoablative tissue removal, and wound healing as aggregate biomechanical insults to the full thickness of the postoperative cornea within the ablation zone diameter. In modeling this elastic property change as a generalized zone of injury and repair without a separate modeling of the flap, the changes in properties within the flap, within the residual stromal bed, and at the flap interface have been combined into a single parameter. Modeling the discrete contributions of the flap and tissue to the overall elastic property change is possible with the current model but would require spatially resolved knowledge of the differential mechanical property effects of LASIK within and deep to the flap. Continued development of in vivo techniques for characterizing corneal material properties in three dimensions [43] will be important for patient-specific surgical optimization and avoidance of ex vivo estimates since relatively fine control of flap dimensions and excimer laser photoablation algorithms is possible. However, until such data is available, a zonal injury approach to the problem allows for optimization of a single material property parameter and is adequate for retrospectively assessing the biomechanical impact of LASIK and for producing accurate predictions of postoperative optical outcomes with a model informed only by preoperative clinical measurements and the planned surgical algorithm. Another limitation of this study is that the assumed corneal-scleral relationship can affect the no-load geometry estimated by the inverse FEM procedure. Since in this study, the same no-load configuration was used for pre- and post-LASIK (with tissue removal simulated in the post-LASIK case), it was possible to express the change in elastic properties as a percentage value of the preoperative elastic properties. While the results of cohesive tensile strength testing [42] and the sensitivity analysis performed in this study provide some support for the elastic property change estimates in these simulations, future studies will need to assess the sensitivity of these models to the range of variations in corneal-scleral elastic properties likely to be encountered in patients across a range of ages. Large scale modeling will also allow for the study of the variation in elastic property changes across a wide range of ablation parameters to better assess the impact of such variables on the risk of corneal ectasia.

In addition to material properties and ablation profile, the IOP may influence the shape of the cornea before and especially after corneal surgery and is a potential limitation in patient-specific modeling. The accuracy of the transcorneal IOP measurement is uncertain due to reduced thickness, weakening of the cornea [24–26], and differences in device measurement methods [26–28]. Reduced thickness and weakening lead to underestimated IOP [24]. Studies have compared devices commonly used to measure changes in IOP from pre- to postsurgery [25–28]. Goldmann IOP tends to decrease after ablation due to reduced thickness and weakening, whereas IOP measured by dynamic contour tonometry (Ziemer Ophthalmic Systems AG, Switzerland) is relatively unaffected by thickness [25–28]. Because the IOP_{cc} measured by the ORA is only weakly correlated with CCT [26,33] and is relatively unaffected by LASIK [26,34], we used it as a practical proxy for actual intraocular loading pressure before and after LASIK.

In summary, we present a method for patient-specific 3D computational modeling of corneal refractive surgery that provides representations of clinical corneal shape changes in LASIK and allows inverse estimation of the surgical impact on corneal elastic properties. The FEMs generated in this study take less than 10 min to solve and do not require significant computational resources. Further improvements in meshing size and automation of the 3D model generation can further reduce the solution time. The accuracy of the models will depend on the quality of the clinical geometry data supplied, and the results could therefore be device-specific. While the sensitivity of model accuracy to this potential error is unknown, the use of data obtained from the same instrument before and after surgery minimizes potential confounding effects. Ultimately, an accurate FE model of the corneoscleral complex that can be populated with patient-specific clinical data affords the opportunity to simulate and perhaps refine surgical results in any corneal surgery that affects the cornea's biomechanical state.

Acknowledgment

This study was supported in part by NIH Grant Nos. K12RR023264 and 1KL2RR024990, Challenge and Unrestricted Grants from Research to Prevent Blindness to the Department of Ophthalmology of the Cleveland Clinic Lerner College of Medicine of Case Western Reserve University, and the National Keratoconus Foundation/Discovery Eye Foundation. W.D. is a recipient of a Research to Prevent Blindness Career Development Award.

References

[1] Solomon, K. D., Fernández de Castro, L. E., Sandoval, H. P., Biber, J. M., Groat, B., Neff, K. D., Ying, M. S., French, J. W., Donnenfeld, E. D., Lindstrom, R. L., and Joint LASIK Study Task Force, 2009, "LASIK World Literature Review: Quality of Life and Patient Satisfaction," Ophthalmology, **116**(4), pp. 691–701.

[2] Kosaki, R., Maeda, N., Hayashi, H., Fujikado, T., and Okamoto, S., 2009, "Effect of NIDEK Optimized Aspheric Transition Zone Ablation Profile on Higher Order Aberrations During LASIK for Myopia," J. Refract. Surg., **25**(4), pp. 331–338.

[3] Randleman, J. B., White, A. J., Jr., Lynn, M. J., Hu, M. H., and Stulting, R. D., 2009, "Incidence, Outcomes, and Risk Factors for Retreatment After Wavefront-Optimized Ablations With PRK and LASIK," J. Refract. Surg., **25**(3), pp. 273–276.

[4] Netto, M. V., Dupps, W. J., and Wilson, S. E., 2006, "Wavefront-Guided Ablation: Evidence for Efficacy Compared to Traditional Ablation," Am. J. Ophthalmol., **141**(2), pp. 360–368.

[5] Schallhorn, S. C., Farjo, A. A., Huang, D., Boxer Wachler, B. S., Trattler, W. B., Tanzer, D. J., Majmudar, P. A., and Sugar, A., 2008, "Wavefront-Guided LASIK for the Correction of Primary Myopia and Astigmatism: A Report by the American Academy of Ophthalmology," Ophthalmology, **115**(7), pp. 1249–1261.

[6] Cano, D., Barbero, S., and Marcos, S., 2004, "Comparison of Real and Computer-Simulated Outcomes of LASIK Refractive Surgery," J. Opt. Soc. Am. A Opt. Image Sci. Vis, **21**(6), pp. 926–936.

[7] Dupps, W. J., and Roberts, C., 2001, "Effect of Acute Biomechanical Changes on Corneal Curvature After Photokeratectomy," J. Refract. Surg., **17**, pp. 658–669.

[8] Roberts, C., 2002, "Biomechanics of the Cornea and Wavefront-Guided Laser Refractive Surgery," J. Refract. Surg., **18**, pp. S589–S592.

[9] Dorronsoro, C., Cano, D., Merayo-Lloves, J., and Marcos, S., 2006, "Experiments on PMMA Models to Predict the Impact of Corneal Refractive Surgery on Corneal Shape," Opt. Express, **14**(13), pp. 6142–56.

[10] Marcos, S., Cano, D., and Barbero, S., 2003, "Increase in Corneal Asphericity After Standard Laser In Situ Keratomileusis for Myopia Is Not Inherent to the Munnerlyn Algorithm," J. Refract. Surg., **19**(5), pp. S592–S596.

[11] Potgieter, F. J., Roberts, C., Cox, I. G., Mahmoud, A. M., Herderick, E. E., Roetz, M., and Steenkamp, W., 2005, "Prediction of Flap Response," J. Cataract Refractive Surg., **31**(1), pp. 106–114.

[12] Krueger, R. R., and Dupps, W. J., 2007, "Biomechanical Effects of Femtosecond and Microkeratome-Based Flap Creation: Prospective Contralateral Examination of Two Patients," J. Refract. Surg., **23**(8), pp. 800–807.

[13] Sinha Roy, A., and Dupps, W. J., Jr., 2009, "Effects of Altered Corneal Stiffness on Native and Postoperative LASIK Corneal Biomechanical Behavior: A Whole-Eye Finite Element Analysis," J. Refract. Surg., **25**(10), pp. 875–887.

[14] Alastrué, V., Calvo, B., Peña, E., and Doblaré, M., 2006, "Biomechanical Modeling of Refractive Corneal Surgery," ASME J. Biomech. Eng., **128**(1), pp. 150–160.

[15] Deenadayalu, C., Mobasher, B., Rajan, S. D., and Hall, G. W., 2006, "Refractive Change Induced by the LASIK Flap in a Biomechanical Finite Element Model," J. Refract. Surg., **22**(3), pp. 286–292.

[16] Pandolfi, A., and Holzapfel, G. A., 2008, "Three-Dimensional Modeling and Computational Analysis of the Human Cornea Considering Distributed Collagen Fibril Orientations," ASME J. Biomech. Eng., **130**(6), p. 061006.

[17] Navarro, R., Palos, F., Lanchares, E., Calvo, B., and Cristóbal, J. A., 2009,

"Lower- and Higher-Order Aberrations Predicted by an Optomechanical Model of Arcuate Keratotomy for Astigmatism," J. Cataract Refractive Surg., **35**(1), pp. 158–165.
[18] Munnerlyn, C. R., Koons, S. J., and Marshall, J., 1988, "Photorefractive Keratectomy: A Technique for Laser Refractive Surgery," J. Cataract Refractive Surg., **14**, pp. 46–52.
[19] Mrochen, M., Donitzky, C., Wüllner, C., and Löffler, J., 2004, "Wavefront-Optimized Ablation Profiles: Theoretical Background," J. Cataract Refractive Surg., **30**(4), pp. 775–785.
[20] Koller, T., Iseli, H. P., Hafezi, F., Mrochen, M., and Seiler, T., 2006, "Q-factor Customized Ablation Profile for the Correction of Myopic Astigmatism," J. Çataract Refractive Surg., **32**(4), pp. 584–589.
[21] Śródka, W., and Iskander, D. R., 2008, "Optically Inspired Biomechanical Model of the Human Eyeball," J. Biomed. Opt., **13**(4), p. 044034.
[22] Amini, R., and Barocas, V. H., 2009 "Anterior Chamber Angle Opening During Corneoscleral Indentation: The Mechanism of Whole Eye Globe Deformation and the Importance of the Limbus," Invest. Ophthalmol. Visual Sci., **50**, pp. 5288–5294.
[23] Boyce, B. L., Grazier, J. M., Jones, R. E., and Nguyen, T. D., 2008, "Full-field Deformation of Bovine Cornea Under Constrained Inflation Conditions," Biomaterials, **29**(28), pp. 3896–3904.
[24] Liu, J., and Roberts, C. J., 2005, "Influence of Corneal Biomechanical Properties on Intraocular Pressure Measurement: Quantitative Analysis," J. Cataract Refractive Surg., **31**(1), pp. 146–155.
[25] Pepose, J. S., Feigenbaum, S. K., Qazi, M. A., Sanderson, J. P., and Roberts, C. J., 2007, "Changes in Corneal Biomechanics and Intraocular Pressure Following LASIK Using Static, Dynamic, and Noncontact Tonometry," Am. J. Ophthalmol., **143**(1), pp. 39–47.
[26] Kirwan, C., and O'Keefe, M., 2008, "Measurement of Intraocular Pressure in LASIK and LASEK Patients Using the Reichert Ocular Response Analyzer and Goldmann Applanation Tonometry," J. Refract. Surg., **24**(4), pp. 366–370.
[27] Bayraktar, S., and Bayraktar, Z., 2005, "Central Corneal Thickness and Intraocular Pressure Relationship in Eyes With and Without Previous LASIK: Comparison of Goldmann Applanation Tonometer With Pneumatonometer," Eur. J. Ophthalmol., **15**(1), pp. 81–88.
[28] Kaufmann, C., Bachmann, L. M., and Thiel, M. A., 2003, "Intraocular Pressure Measurements Using Dynamic Contour Tonometry After Laser In Situ Keratomileusis," Invest. Ophthalmol. Visual Sci., **44**(9), pp. 3790–3794.
[29] Elsheikh, A., Brown, M., Alhasso, D., Rama, P., Campanelli, M., and Garway-Heath, D., 2008, "Experimental Assessment of Corneal Anisotropy," J. Refract. Surg., **24**(2), pp. 178–187.
[30] Dupps, W. J., Jr., Netto, M. V., Herekar, S., and Krueger, R. R., 2007, "Surface Wave Elastometry of the Cornea in Porcine and Human Donor Eyes," J. Refract. Surg., **23**(1), pp. 66–75.
[31] Thornton, I. L., Dupps, W. J., Roy, A. S., and Krueger, R. R., 2009, "Biomechanical Effects of Intraocular Pressure Elevation on Optic Nerve/Lamina Cribrosa Before and After Peripapillary Scleral Collagen Cross-Linking," Invest. Ophthalmol. Visual Sci., **50**(3), pp. 1227–1233.
[32] Sarver, E. J., 2006, "Calculation of Corneal Spherical Aberration for Aspheric IOL Selection," Refractive Surgery 2006: The Times They Are A-Changin, American Academy of Ophthalmology.
[33] Qazi, M. A., Sanderson, J. P., Mahmoud, A. M., Yoon, E. Y., Roberts, C. J., and Pepose, J. S., 2009, "Postoperative Changes in Intraocular Pressure and Corneal Biomechanical Metrics Laser In Situ Keratomileusis Versus Laser-Assisted Subepithelial Keratectomy," J. Cataract Refractive Surg., **35**(10), pp. 1774–1788.
[34] Kotecha, A., Elsheikh, A., Roberts, C. R., Zhu, H., and Garway-Heath, D. F., 2006, "Corneal Thickness- and Age-Related Biomechanical Properties of the Cornea Measured With the Ocular Response Analyzer," Invest. Ophthalmol. Visual Sci., **47**(12), pp. 5337–5347.
[35] Shah, S., Laiquzzaman, M., Yeung, I., Pan, X., and Roberts, C., 2009, "The Use of the Ocular Response Analyser to Determine Corneal Hysteresis in Eyes Before and After Excimer Laser Refractive Surgery," Contact Lens & Anterior Eye, **32**(3), pp. 123–128.
[36] Ortiz, D., Piñero, D., Shabayek, M. H., Arnalich-Montiel, F., and Alió, J. L., 2007, "Corneal Biomechanical Properties in Normal, Post-Laser In Situ Keratomileusis, and Keratoconic Eyes," J. Cataract Refractive Surg., **33**(8), pp. 1371–1375.
[37] Kirwan, C., and O'Keefe, M., 2008, "Corneal Hysteresis Using the Reichert Ocular Response Analyser: Findings Pre- and Post-LASIK and LASEK," Acta Ophthalmologica, **86**(2), pp. 215–218.
[38] Dupps, W. J., 2007, "Hysteresis: New Mechanospeak for the Ophthalmologist," J. Cataract Refractive Surg., **33**(9), pp. 1499–1501.
[39] Glass, D. H., Roberts, C. J., Litsky, A. S., and Weber, P. A., 2008, "A Viscoelastic Biomechanical Model of the Cornea Describing the Effect of Viscosity and Elasticity on Hysteresis," Invest. Ophthalmol. Visual Sci., **49**(9), pp. 3919–3926.
[40] de Medeiros, F. W., Sinha-Roy, A., Alves, M. R., Wilson, S. E., and Dupps, W. J., Jr., 2010, "Differences in the Early Biomechanical Effects of Hyperopic and Myopic Laser in situ Keratomileusis," J. Cataract Refractive Surg., **36**(6), pp. 947–953.
[41] Dupps, W. J., Jr., and Wilson, S. E., 2006, "Biomechanics and Wound Healing in the Cornea," Exp. Eye Res., **83**(4), pp. 709–720.
[42] Schmack, I., Dawson, D. G., McCarey, B. E., Waring, G. O., III, Grossniklaus, H. E., and Edelhauser, H. F., 2005, "Cohesive Tensile Strength of Human LASIK Wounds With Histologic, Ultrastructural, and Clinical Correlations," J. Refract. Surg., **21**(5), pp. 433–45.
[43] Ford, M., Dupps, W. J., Huprikar, N., Lin, R., and Rollins, A. M., 2006, "OCT Elastography by Pressure-Induced Optical Feature Flow. Progress in Biomedical Optics and Imaging," Proceedings of SPIE, Paper No. 6138OP.